

Projecting non-diffracting waves with intermediate-plane holography

Argha Mondal, Aaron Yevick, Lauren C. Blackburn, Nikitas Kanellakopoulos, and David G. Grier
Department of Physics and Center for Soft Matter Research, New York University, New York, NY 10003

We introduce an approach to phase-only holography that substantially improves the ability of holographic trapping systems to project propagation-invariant modes of light. This technique is particularly well suited for projecting accelerating modes and long-range tractor beams.

Structuring laser beams with computer-generated holograms has revolutionized optical micromanipulation [1] and optical communication [2–4]. Using holograms to project propagation-invariant modes of light, for example, has led to the remarkable discovery that some non-diffracting modes can act as tractor beams, pulling illuminated objects upstream rather than trapping them or pushing them downstream [5, 6]. Applications of tractor beams and other exotic light modes have been hampered by the poor diffraction efficiency of the holograms used to project them, which can be less than 10^{-3} [7, 8]. To address this problem, we introduce intermediate-plane holography, a technique that relaxes constraints typically employed in the holographic trapping technique [1], to improve both diffraction efficiency and mode purity. We illustrate these capabilities by projecting Bessel beams, which constitute the natural basis for propagation-invariant modes [9, 10]. We then use these techniques to project meter-long optical conveyors [7, 8, 11] and solenoid beams [6, 12], which are tractor-beam modes composed of superpositions of Bessel beams. These experiments demonstrate a 400-fold improvement in diffraction efficiency relative to the standard holographic optical trapping technique, and a 1000-fold increase in non-diffracting range.

Holograms intended for optical micromanipulation typically are designed to modify the phase profile of an incident laser beam, but not the amplitude. The phase-only hologram then propagates to a converging lens that transforms it into the intended mode. Scalar diffraction theory approximates this transformation as a Fourier transform [13]. Difficulties are encountered when the Fourier transform of the desired mode features amplitude variations that can not be encoded naturally in a phase-only diffractive optical element.

For example, the ideal complex-valued hologram encoding an m -th order Bessel beam takes the form of an infinitesimally fine ring,

$$E_{\alpha,m}(\mathbf{r}, 0) = \delta(r - R_\alpha) e^{im\theta}, \quad (1)$$

whose radius, $R_\alpha = f \tan \alpha$, depends on the focal length of the projecting lens, f , and the desired convergence angle of the Bessel beam, α . Equation (1) expresses the scalar field in terms of the two-dimensional polar coordinates, $\mathbf{r} = (r, \theta)$, in the plane $z = 0$. More generally, $E_{\alpha,m}(\mathbf{r}, z)$ describes transverse profile of the same field at axial position z .

The ideal ring hologram consists of an amplitude mask, shown schematically in Fig. 1(a), that only allows light to pass through the thin annulus at radius R_α , and a phase mask that imposes a helical pitch on the transmitted wavefronts. The same effect can be achieved with a phase-only hologram,

$$\varphi_{\alpha,m}(\mathbf{r}) = \begin{cases} m\theta \bmod 2\pi, & r = R_\alpha \\ \varphi_0(\mathbf{r}), & \text{otherwise} \end{cases} \quad (2)$$

where $\varphi_0(\mathbf{r})$ is an undetermined phase function that diverts light away from the optical axis [14].

Equation (2) poses two substantial problems for standard holographic trapping implementations of the kind represented in Fig. 1(a). In the first place, the delta-function amplitude profile in the hologram plane cannot be encoded faithfully on a pixellated diffractive optical element. The bright ring in Fig. 1(a) represents the intensity, $I(\mathbf{r}, 0) = |E_{\alpha,0}(\mathbf{r}, 0)|^2$, projected by an $m = 0$ ring hologram, treated as an ideal amplitude mask. The ring's finite thickness arises from the mask's finite pixel size. Rather than projecting a wave with a single value of α , this finite-thickness ring constitutes a superposition of ring holograms that corresponds to a superposition of Bessel beams with a range of convergence angles, α . Interference among these superposed modes causes periodic axial intensity variations, and so limits the propagation-invariant range of the superposition [7]. In the second place, only a few pixels in the hologram plane contribute to the intended Bessel beam. The rest of the hologram's area is dedicated to the phase function $\varphi_0(\mathbf{r})$ that diverts extraneous light away from the desired mode. Pixellated ring holograms thus suffer from a combination of poor mode fidelity and extremely poor diffraction efficiency.

Both deficiencies can be mitigated by considering light's propagation from the hologram plane to the converging lens. The field at distance z along the optical axis may be estimated with the Rayleigh-Sommerfeld diffraction integral [15],

$$E(\mathbf{r}, z) = \int \tilde{E}(\mathbf{q}, 0) \tilde{H}_z(\mathbf{q}) e^{-i\mathbf{q} \cdot \mathbf{r}} d^2 q, \quad (3a)$$

where $\tilde{E}(\mathbf{q}, 0)$ is the two-dimensional Fourier transform of the field $E(\mathbf{r}, 0)$ in the plane $z = 0$ and

$$\tilde{H}_z(\mathbf{q}) = e^{iz\sqrt{k^2 - q^2}} \quad (3b)$$

is the Fourier transform of the Rayleigh-Sommerfeld propagator for light of wave number k [13]. Because the light diffracts as it propagates, challenging amplitude variations in $E(\mathbf{r}, 0)$ can be substantially less pronounced in the intermediate plane at axial position z . This can be seen in the intermediate-plane intensity, $I(\mathbf{r}, z) = |E_{\alpha,0}(\mathbf{r}, z)|^2$, for the $m = 0$ mode in Fig. 1(a). A phase-only hologram designed for this plane therefore will have much better diffraction efficiency than the ideal hologram designed for $z = 0$. Indeed, the location, z , of the intermediate plane can be selected to maximize this benefit. Improving diffraction efficiency naturally improves mode fidelity by reducing the amount of light in unwanted modes. Performance may be even better than this observation suggests because $E(\mathbf{r}, z)$ is computed from the ideal field, without compromise for pixelation.

The phase-only intermediate-plane hologram associated with $E(\mathbf{r}, 0)$ may be approximated by the phase, $\varphi(\mathbf{r}, z)$, of $E(\mathbf{r}, z)$, ignoring amplitude variations. The intermediate-plane phase for the $m = 0$ Bessel beam is presented in Fig. 1(b). If necessary, some accommodation may be made for remaining amplitude variations through any of the techniques that have been developed for encoding complex-valued fields on phase-only diffractive optical elements [14]. In practice, this often is unnecessary, and the phase of the computed intermediate-plane field often serves as a mode-forming hologram with high diffraction efficiency.

The benefits of intermediate-plane holography come at a cost. Specifically, the diffractive optical element no longer is located in the focal plane of the projecting lens. This requires modifying the optical layout of a typical holographic trapping system. For the particular case of reflective holograms, space constraints may limit the range of z , and thus the benefit of the technique. In cases where large positive values of z are physically inaccessible, negative values may offer the same benefits while affording sufficient space for practical implementation.

Setting $z = f$ addresses these geometric considerations by placing the intermediate-plane hologram in the same plane as the converging lens. The associated parabolic phase profile,

$$\varphi_f(\mathbf{r}) = \frac{\pi r^2}{\lambda f} \bmod 2\pi, \quad (4)$$

can be integrated into the phase function for the intermediate-plane hologram,

$$\varphi(\mathbf{r}) = [\varphi(\mathbf{r}, f) + \varphi_f(\mathbf{r})] \bmod 2\pi, \quad (5)$$

thereby eliminating the need for the physical lens altogether. This mode of operation is presented in Fig. 1(c) and is the approach we will adopt for experimental demonstrations.

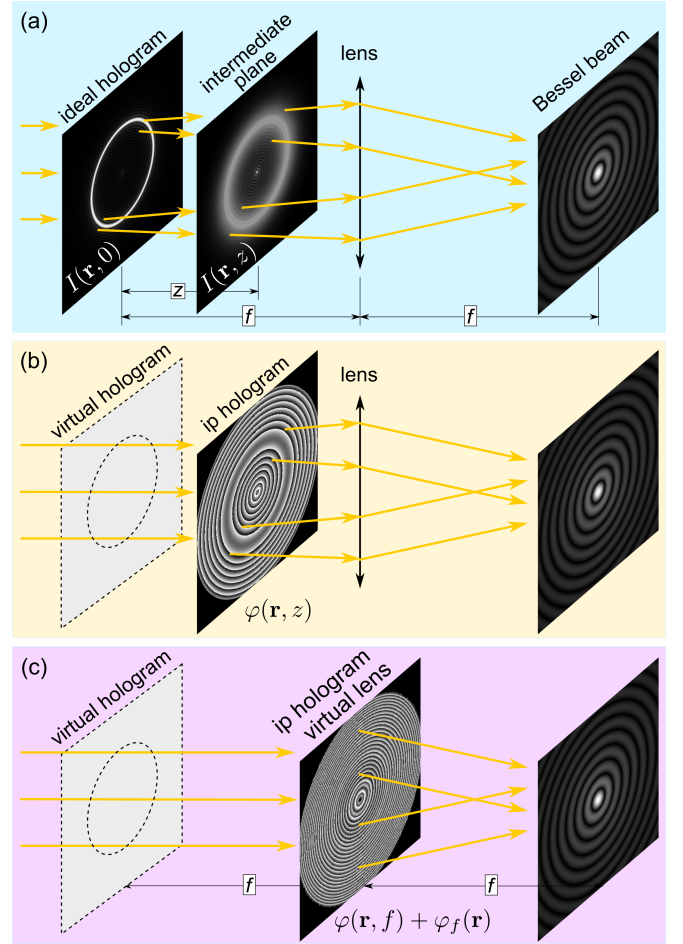


FIG. 1. Intermediate-plane holography. (a) Conventional holographic projection of a Bessel beam. The field diffracted by a ring hologram propagates to a converging lens of focal length f that projects it into the non-diffracting mode. (b) A phase-only hologram in an intermediate plane recreates the ring-hologram's wavefront structure at substantially higher diffraction efficiency. (c) Moving the intermediate plane to $z = f$ and incorporating the phase function for a converging lens of focal length f creates a mode converter that projects the Bessel beam directly.

For the particular case of a Bessel beam, the Fourier transform of the ideal ring hologram is

$$\tilde{E}_{\alpha,m}(\mathbf{q}, 0) = J_m(qR_\alpha) e^{im\theta}. \quad (6)$$

Applying Eq. (3) then yields an expression for the field in the intermediate plane,

$$E_{\alpha,m}(\mathbf{r}, z) = e^{im\theta} \int_0^k q J_m(qr) J_m(qR_\alpha) e^{iz\sqrt{k^2 - q^2}} dq, \quad (7)$$

whose phase is the first-order approximation to the intermediate-plane phase hologram encoding the Bessel beam. The upper limit of integration in Eq. (7) ignores exponentially small contributions from terms with $q > k$ because $kz \gg 1$ in practice.

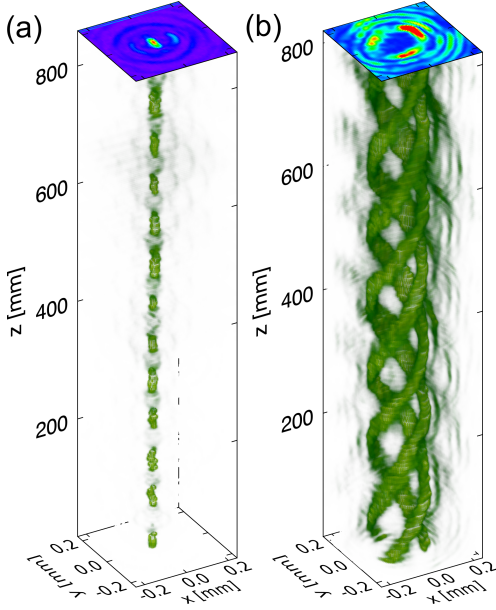


FIG. 2. Tractor-beam modes projected with intermediate-plane holograms.

Equation (7) can be computed numerically for arbitrary α and m . In the limit $z \gg R_\alpha$, it reduces to

$$E_{\alpha,m}(\mathbf{r}, z) \approx \beta^2 e^{-i \frac{kr^2}{2z}} e^{ikR_\alpha(\beta + \frac{1}{\beta})} J_m(\beta kr) e^{im\theta}, \quad (8)$$

$$\text{where } \beta = \frac{R_\alpha}{\sqrt{r^2 + z^2}}. \quad (9)$$

The single-element mode converter,

$$E_{\alpha,m}(\mathbf{r}) = E_{\alpha,m}(\mathbf{r}, f) e^{i\varphi_f(\mathbf{r})}, \quad (10)$$

has a phase profile that, in turn, reduces to the conical profile of an axicon in the long-range limit, $z \gg R_\alpha$. The difference for shorter ranges can reduce the mode purity and non-diffracting range of beams projected with axicons relative to those projected with intermediate-plane holograms.

Superpositions of Bessel beams can be obtained by superposing results of the form predicted by Eq. (10) [16]. These are particularly useful for projecting tractor beams. The field for an optical conveyor [7, 8, 11], for example, can be as simple as a two-fold superposition of equal-helicity Bessel beams:

$$E_{\alpha,m}^{\delta\alpha}(\mathbf{r}, \phi) = E_{\alpha,m}(\mathbf{r}) + e^{i\phi} E_{\alpha+\delta\alpha,m}(\mathbf{r}). \quad (11)$$

An example with $m = 0$, $\alpha = 5 \times 10^{-3}$ rad and $\delta\alpha = 1 \times 10^{-4}$ rad is presented in Fig. 2(a). This linearly polarized beam was created at $\lambda = 532$ nm (Coherent Verdi 5W) using a phase-only spatial light modulator (SLM, Hamamatsu X10468-16) to imprint the phase of the field described by Eq. (11) on the collimated beam's wavefronts. This beam's axial intensity profile is characterized by a periodic array of maxima spaced by $\Delta z =$

$\lambda[\tan(\alpha + \delta\alpha) - \tan \alpha]^{-1}$. The alternating intensity maxima and minima act as traps for illuminated objects that can be moved along the beam's axis by varying the relative phase, ϕ [7, 8, 11].

The beam's intensity profile was measured by moving a standard video camera (NEC TI-324AII) along an optical rail in 5 mm increments. The resulting stack of transverse slices then was combined into a volumetric data set with $6.4 \mu\text{m}$ transverse spatial resolution. The transverse width of the intensity maxima does not change appreciably over a range of 2 m. Figure 2 is limited to a range of 0.8 m for clarity.

Images were recorded with a total beam power of 3 mW, as recorded by an optical power meter (Coherent Lasermate). The upper limit of the conveyor beam's power, 1 W, was set by the 3 W limit of the SLM, with a total diffraction efficiency of 0.3 into the desired mode. This represents a factor of 400 improvement of diffraction efficiency relative to a standard ring hologram [7, 8] given the SLM's 800×600 array of phase pixels. The beam's non-diffracting range exceeds that of previously reported holographically-projected conveyor modes [7, 8] by a factor of more than 10^3 .

Intermediate-plane holography particularly useful for projecting more sophisticated superpositions of Bessel beams, such as the solenoidal wave presented in Fig. 2(b). This two-beam superposition has the general form

$$E_{\alpha,m}^\mu(\mathbf{r}) = E_{\alpha,m}(\mathbf{r}) + \frac{J_m(j'_{m,2})}{J_{m'}(j'_{m',1})} E_{\alpha',m'}(\mathbf{r}), \quad (12)$$

where $m' = m + \mu$, $\alpha' = (j'_{m,2}/j'_{m',1})\alpha$, and $j'_{m,n}$ is the n -th zero of $J'_m(x)$. The particular realization in Fig. 2(b) is a three-fold ($\mu = 3$) tractor-beam mode [12] with $m = 10$ and $\alpha = 10^{-3}$ rad. These parameters satisfy the condition $\cos(\alpha) > [m/(m + \mu)] \cos(\alpha + \delta\alpha)$ required for a solenoidal wave to act as a tractor beam [12]. As for the conveyor beam, the intermediate-plane hologram projecting the solenoidal tractor beam has a diffraction efficiency of roughly 0.3, and yields a non-diffracting range exceeding 1 m.

Solenoidal modes are examples of accelerating waves [17] in the sense that the position of the principal intensity maximum, is a non-linear function of axial position. Intermediate-plane holography therefore is useful for creating non-diffracting accelerating modes with high diffraction efficiency.

The same approach used for these demonstrations also can be applied to more complicated superpositions of Bessel modes [6, 18–20]. In all cases, the intermediate-plane approach should provide better mode purity, longer range and higher diffraction efficiency than conventional holographic mode-conversion techniques.

In addition to projecting collimated modes, intermediate-plane holograms can project waves that converge or diverge at a specified rate. This is

achieved by deliberately mis-matching the placement of the intermediate plane with the back focal plane of the converging element. For intermediate-plane holograms with integrated converging phase profiles, this is achieved by having the displacement, z , differ from the focal length f . In that case, the resulting divergence angle is $\gamma = \tan^{-1}(1 - z/f)$. Each superposed mode in such an element, furthermore, can have a different divergence angle.

Intermediate-plane holography is particularly useful for projecting modes whose ideal Fresnel holograms are dominated by large amplitude variations, and so suffer from low diffraction efficiency. In addition to improving diffraction efficiency, shifting the hologram plane also can improve mode purity by moving the length scale for phase variations into the spatial bandwidth of a practical diffractive optical element. Both of these element figure in the success of intermediate-plane holograms for projecting Bessel beams and their superpositions. Because Bessel beams are the natural basis for propagation-invariant modes, intermediate-plane holography lends itself naturally to long-range projection. We have demonstrated meter-scale projection using centimeter-scale optical elements. These same elements have additional potential applications for topologically multiplexing and de-multiplexing non-diffracting modes for optical communications [2–4]. The same ability to project sophisticated superpositions of topological modes could have additional applications to remote sensing and LIDAR [21]. Finally, the same principals discussed here in the context of optical holography should apply equally well to other types of waves, most notably to acoustic waves.

This work was supported primarily by the National Science Foundation through Award no. DMR-1305875 and in part by NASA through Award no. NNX13AK76G and through the NASA Space Technology Research Fellowship (NSTRF) program under Award no. NN14AQ40H.

Tur, Poul Kristensen, Hao Huang, Alan E Willner, and Siddharth Ramachandran, “Terabit-scale orbital angular momentum mode division multiplexing in fibers,” *Science* **340**, 1545–1548 (2013).

- [4] Alan E Willner, Hao Huang, Yan Yan, Yongxiong Ren, Nisar Ahmed, Goudong Xie, Changjing Bao, L Li, Y Cao, Z Zhao, *et al.*, “Optical communications using orbital angular momentum beams,” *Advances in Optics and Photonics* **7**, 66–106 (2015).
- [5] Philip L. Marston, “Axial radiation force of a Bessel beam on a sphere and direction reversal of the force,” *J. Acoust. Soc. Am.* **120**, 3518–3524 (2006).
- [6] Sang-Hyuk Lee, Yohai Roichman, and David G. Grier, “Optical solenoid beams,” *Opt. Express* **18**, 6988–6993 (2010).
- [7] David B. Ruffner and David G. Grier, “Optical conveyors: A class of active tractor beams,” *Phys. Rev. Lett.* **109**, 163903 (2012).
- [8] David B. Ruffner and David G. Grier, “Universal, strong and long-ranged trapping by optical conveyors,” *Opt. Express* **22**, 26834–26853 (2014).
- [9] J. Durnin, “Exact-solutions for nondiffracting beams. 1. the scalar theory,” *J. Opt. Soc. Am. A* **4**, 651–654 (1987).
- [10] J. Durnin, J. J. Miceli, Jr., and J. H. Eberly, “Diffraction-free beams,” *Phys. Rev. Lett.* **58**, 1499–1501 (1987).
- [11] Tomáš Čižmar, Veneranda Garcés-Chávez, Kishan Dholakia, and Pavel Zemánek, “Optical conveyor belt for delivery of submicron objects,” *Appl. Phys. Lett.* **86**, 174101 (2005).
- [12] Aaron Yevick, David B. Ruffner, and David G. Grier, “Tractor beams in the Rayleigh limit,” *Phys. Rev. A* **93**, 043807 (2016).
- [13] Joseph W. Goodman, *Introduction to Fourier Optics*, 3rd ed. (McGraw-Hill, New York, 2005).
- [14] Yohai Roichman and David G. Grier, “Projecting extended optical traps with shape-phase holography,” *Opt. Lett.* **31**, 1675–1677 (2006).
- [15] Max Born and Emil Wolf, *Principles of Optics*, 7th ed. (Cambridge University Press, Cambridge, 1999).
- [16] D. McGloin, V. Garcés-Chávez, and K. Dholakia, “Interfering Bessel beams for optical micromanipulation,” *Opt. Lett.* **28**, 657–659 (2003).
- [17] M. V. Berry and N. L. Balazs, “Nonspreadng wave packets,” *Am. J. Phys.* **47**, 264–267 (1979).
- [18] Tomáš Čižmár and Kishan Dholakia, “Tunable Bessel light modes: engineering the axial propagation,” *Opt. Express* **17**, 15558–15570 (2009).
- [19] Ruslan Vasilyeu, Angela Dudley, Nikolai Khilo, and Andrew Forbes, “Generating superpositions of higher-order Bessel beams,” *Opt. Express* **17**, 23389–23395 (2009).
- [20] Igor A. Litvin, Angela Dudley, and Andrew Forbes, “Poynting vector and orbital angular momentum density of superpositions of Bessel beams,” *Opt. Express* **19**, 16760–16771 (2011).
- [21] Neda Cvijetic, Giovanni Milione, Ezra Ip, and Ting Wang, “Detecting lateral motion using lights orbital angular momentum,” *Sci. Rep.* **5**, 15422 (2015).

-
- [1] David G. Grier, “A revolution in optical manipulation,” *Nature* **424**, 810–816 (2003).
 - [2] Graham Gibson, Johannes Courtial, Miles J Padgett, Mikhail Vasnetsov, Valeriy Paško, Stephen M Barnett, and Sonja Franke-Arnold, “Free-space information transfer using light beams carrying orbital angular momentum,” *Opt. Express* **12**, 5448–5456 (2004).
 - [3] Nenad Bozinovic, Yang Yue, Yongxiong Ren, Moshe